CHARGE ORDERING IN TWISTED BILAYER GRAPHENE MODELED BY A HUBBARD-LIKE HAMILTONIAN, SUPPLEMENTED WITH LONG-RANGE DENSITY–DENSITY INTERACTIONS*

Andrzej Biborski

Academic Centre for Materials and Nanotechnology
AGH University of Krakow
Al. Mickiewicza 30, 30-059 Kraków, Poland

Received 16 February 2026, accepted 16 March 2026, published online 15 May 2026

Moiré systems, such as twisted bilayer graphene or coupled layers of transition metal dichalcogenides, are considered intriguing platforms for understanding a variety of phenomena observed in strongly correlated electron systems. Here, we apply the four-band lattice model of twisted bilayer graphene to analyze whether, in the undoped case, the range of density–density interactions influences the resultant charge ordering. By using semi-classical simulated annealing optimization, as well as unrestricted Hartree–Fock calculations, we show that the pattern of order clearly depends on the range of interaction terms assumed; by performing the energy scaling with the increasing range of interactions taken into account, we select two patterns that possibly refer to the optimal charge distribution at doping $\nu = 0$ — that is, at charge neutrality in the real system.

DOI:10.5506/APhysPolB.57.5-A17

1. Introduction

The moiré systems emerge by combining at least two layers of two-dimensional materials that are twisted with respect to each other or that differ by structural or chemical properties [1, 2]. The archetypal example of such a system is twisted bilayer graphene (TBG) [2–7], in which, at the so-called *magic angles*, narrow bands (or *minibands*) with an energy scale of the order of meV are formed, resulting in the strongly correlated nature of itinerant carriers. This correlated nature of TBG has been an attractive factor in theoretical studies concerning the construction of minimal low-energy models for the narrow bands [8–12], the Mott insulating state

* Presented at the Concepts in Strongly Correlated Quantum Matter Conference (CSCQM), Kraków, Poland, 20–22 November, 2025.

[13–16], and superconductivity, which is supposed to be of unconventional character [17, 18]. Furthermore, moiré structures constituted from transition metal dichalcogenides (TMD), which are currently being extensively studied both experimentally and through theoretical approaches, appear to be a promising platform for understanding major questions related to strongly correlated systems [19]. Indeed, the formation of a Mott insulating state, unconventional superconductivity, and the observation of exotic spin and charge ordering have been experimentally confirmed [20–24] in these materials, as well as studied in terms of theoretical approaches, *e.g.* [25–30]. While the formation of charge order at fillings related to gap opening is well recognized both experimentally and through theoretical investigations for the TMD moiré lattices such as WSe_2/WS_2 heterobilayers, the same is not well identified for TBG. Namely, the electron–electron interactions in TBG are believed to be long ranged, but local Coulombic interactions (*e.g.*, Hubbard U amplitude) clearly dominate. Thus, the natural question regarding the implications of these interactions arises.

In this paper, we implement a Hubbard-like model of TBG at the magic angle, supplied with interaction and hopping amplitudes evaluated by Koshino *et al.* [9]. We systematically increase the long-range Coulomb interactions, showing that the resulting charge order at filling $\nu = 0$ — that is, at a neutrally charged system — depends on the assumed density–density interaction cut-off. In the following, we briefly present the model Hamiltonian of TBG employed. Subsequently, we describe the numerical approaches utilized, present the main results, and summarize our findings in the last section.

2. Model and method

2.1. Hamiltonian

In our investigations, we apply the four-band Hubbard-like model based on findings reported in [9], that is, the electronic Hamiltonian is taken as

$$\hat{\mathcal{H}} = \hat{\mathcal{H}}_0 + \hat{\mathcal{H}}^Z_{ee}\,, \tag{1}$$

where $\mathcal{H}_0$ is the free-electron four-band kinetic term, and $\hat{\mathcal{H}}^Z_{ee}$ contains density–density interactions up to the Z^{th} neighboring site. This Hamiltonian model effectively maps the TBG moiré structure to the two valley states $\xi \in \{\alpha, \beta\}$ on each site $\{\mu, \nu\}$, where $\mu, \nu \in A \cup B$ with A, B labels the sets of indices belonging to the two interpenetrating triangular sub-lattices that ultimately form the honeycomb structure. That is,

$$\hat{\mathcal{H}}_0 = \sum_{\mu,\nu} \sum_{\xi} \sum_{\sigma} t^{\xi}_{\mu\nu} \hat{a}^{\dagger}_{\mu,\xi,\sigma} \hat{a}_{\nu,\xi,\sigma}\,, \tag{2}$$

where $\sigma = \{\uparrow, \downarrow\}$ indicates the z^{th} component of spin, and $t^{\xi}_{\mu\nu}$ denotes the hopping amplitudes. Note that valley degrees of freedom are encoded in complex conjugation for hoppings between two sites; that is $t^{\alpha}_{\mu\nu} = (t^{\beta}_{\mu\nu})^*$. The operator $\hat{a}_{\nu,\xi,\sigma}(\hat{a}^{\dagger}_{\nu,\xi,\sigma})$ is a standard annihilation (creation) operator conforming to fermionic anti-commutation rules. Note that in $\hat{\mathcal{H}}_0$, we take hoppings up to the 5^{th} neighboring spin-orbital, which is sufficient to describe the band structure of mini-bands (*i.e.*, the moiré bands) of TBG, as shown in [9]. The part of the Hamiltonian concerning electron–electron interactions is

$$\hat{\mathcal{H}}^{Z}_{ee} = \frac{1}{2}\sum_{\mu,\nu}\sum_{\alpha,\beta} V^{\alpha\beta}_{\mu\nu}\left[\hat{n}_{\alpha,\mu}\hat{n}_{\beta,\nu} - \delta_{\mu\nu}\delta_{\alpha\beta}(\hat{n}_{\alpha,\mu,\uparrow}\hat{n}_{\beta,\nu,\downarrow} + \hat{n}_{\alpha,\mu,\downarrow}\hat{n}_{\beta,\nu,\uparrow})\right] , \quad (3)$$

where the summation is extended up to the Z^{th} neighboring site, and $V^{\alpha\beta}_{\mu\nu}$ stands for the amplitude of the interaction. Note that $V^{\alpha\alpha}_{\mu\mu} \equiv U$ is the standard on-site Hubbard repulsion.

2.2. Methods

To characterize the charge order emerging at half-filling, we apply two different approaches. First, as a supplemental method, we use unrestricted Hartree–Fock (HF) calculations in real space to find the approximate ground state of the Hamiltonian. HF is considered a standard approach for electronic systems; therefore, we do not provide details of this widely known mean-field approach, applying it as implemented in the mVMC package [31].

Nonetheless, as the interactions taken into account are considered up to the 36^{th} neighbor, and self-consistent calculations may lead to a local minimum of variational energy, we find it convenient to apply a different *quasi-classical* method. That is, since U/t, and even V/t (for long-range distances) are of the order of magnitude of 10, we may safely neglect the $\hat{\mathcal{H}}_0$ terms in the Hamiltonian. The interaction part $\hat{\mathcal{H}}^{Z}_{ee}$ is then replaced by its classical counterpart. Precisely, we perform "de-quantization" by replacing $\hat{n}_{\alpha,\mu}$ with $n_{\alpha\mu} \in \{\varnothing \uparrow, \downarrow, \uparrow\downarrow\}$; that is, the possible occupation numbers are integers $\varnothing \to 0, \{\uparrow, \downarrow\} \to 1, \uparrow\downarrow \to 2$, which emulate the conformation of Fermi–Dirac statistics. Eventually, the total semi-classical Hamiltonian H^{Z}_{ee} consists of $\hat{\mathcal{H}}^{Z}_{ee}$ with occupation operators replaced by $n_{\alpha,\mu}$ and $n_{\alpha,\mu,\sigma} \in \{\varnothing, \uparrow, \downarrow\}$.

To optimize the energy of H^{Z}_{ee}, we employ *the simulated annealing* (SA) technique, which is regarded as one of the most effective methods for solving optimization problems that are biased by the existence of multiple local minima. That is, the calculations start from a random distribution of $N_e = n_{\uparrow} + n_{\downarrow}$ electrons, assuming that $n_{\uparrow} = n_{\downarrow}$. N_e refers to the total neutral-

charge system described by the density factor ν

$$\nu = \frac{N_e - 2N_\mathrm{s}}{2N_\mathrm{s}}\,, \tag{4}$$

where N_s is the total number of lattice sites. Then, we set *the virtual temperature* factor $\beta \propto 1/T$ and the energy E^Z of the system

$$E^Z = \left\langle H_{ee}^Z \right\rangle = \frac{1}{|\Omega|}\sum_{\omega}^{\Omega} \mathrm{e}^{-\beta H_{ee}(\omega)} H_{ee}(w)\,, \tag{5}$$

where ω denotes an element in the phase space Ω set, which contains all possible electron configurations. Obviously, for the system with $N_s \propto 10^2$ or larger, the direct summation in Eq. (5) is, in practice, impossible since it scales as $\binom{N_\mathrm{s}}{\frac{1}{2}N}^2$ in this case. Therefore, we use a standard approach to estimate E^Z by applying the Monte-Carlo method, that is

$$E^Z \approx \frac{1}{M}\sum_{\omega}^{M} H_{ee}(\omega)\,, \tag{6}$$

where M samples of configurations ω are drawn from the density distribution $\frac{1}{Z}\,\mathrm{e}^{-\beta H_{ee}(\omega)}$. This is performed by generating a Markov chain using the widely known Metropolis–Hastings procedure. That is, the transition probability between the current configuration ω_i and a trial new configuration ω_j is

$$P(\omega_i \to \omega_j) = \min\left[1,\, \mathrm{e}^{-\beta\left[H_{ee}^Z(\omega_j) - H_{ee}^Z(\omega_i)\right]}\right]\,. \tag{7}$$

First, we randomly draw two occupation numbers $n_{\alpha\mu}$ and $n_{\beta\nu}$ at configuration ω_i and also randomly select one of all possible *jumps* that generate configuration ω_j. Then, ΔE^Z is computed, and the transition is accepted when $P(\omega_i \to \omega_j) > r$, where r is a pseudo-random number drawn from the interval $[0, 1)$ according to a uniform distribution. After a sufficient number of trials M, factor β is increased, and the procedure is repeated with the initial state taken as that resulting from the previous sampling. We repeat this procedure until convergence is reached; that is, the resulting configuration from a few subsequently sampled blocks (each with increased β compared to the preceding one) does not change.

3. Results

3.1. Model parameters

As we have mentioned, the parameters, namely the hoppings and density–density Coulomb interactions applied by us, are based on the findings provided in Ref. [9] for the twist angle $\phi = 1.05°$, that is, for *the magic angle*

where narrow bands emerge. We consider hoppings up to $Z = 5$ since this choice efficiently reproduces the narrow band structure in TBG [9]. The absolute hopping amplitudes are at most of the order of 10^{-1} meV, resulting in the formation of narrow bands whose widths do not exceed ~ 10 meV, whereas the values of density–density electron interactions are an order of magnitude greater for the corresponding distances between sites. Since interaction amplitudes are usually given in $e^2/(\epsilon L_M)$, where $L_M \approx 13.42$ nm is the moiré lattice constant, we take the upper limit [32] of the estimated value of the dielectric constant, setting $\epsilon = 8$. As the Wannier orbitals in TBG at the magic angle are characterized by the three-peak structure [9, 11], it has been shown that integrals $V_{\mu\nu}^{\alpha\beta}$ can be nearly exactly approximated by the analytical formulas [9]. Precisely, peaks in the Wannier function describing the ξ-valley orbital on site μ refer to the vertices of an equilateral triangle with side L_M, in such a way that the sites of A and B sub-lattices are located at the center of mass of the corresponding triangle. Note that the triangle representing B site is therefore rotated by 180° with respect to that referring to A site. Let us denote by $\boldsymbol{R}_\mu^i$ the position of the i^{th} vortex of the triangle associated with μ site; then density–density interactions are computable using the formula

$$V_{\mu\nu}^{\alpha\beta} = \frac{(e/3)^2}{4\pi\epsilon_0\epsilon}\left[\sum_{\boldsymbol{R}_\mu^i}\sum_{\boldsymbol{R}_\nu^j\neq\boldsymbol{R}_\mu^i}\frac{1}{\left|\boldsymbol{R}_\mu^i-\boldsymbol{R}_\nu^j\right|}+\sum_{\boldsymbol{R}_\nu^j,\boldsymbol{R}_\mu^i}\delta_{\boldsymbol{R}_\nu^j,\boldsymbol{R}_\mu^i}\frac{1}{0.28L_M}\right]. \tag{8}$$

By applying the above equation, one obtains $U \approx 1.857\frac{e^2}{4\pi\epsilon_0\epsilon}$, which is ≈ 33 meV when $\epsilon = 8$, an order of magnitude greater than the kinetic energy scale. The inter-site interactions are also of substantial magnitude and decay slowly. Namely, assigning interactions between Z^{th} neighbors as V^Z, the nearest-neighbor amplitude is $V^1 \approx 1.524\,\frac{e^2}{4\pi\epsilon_0\epsilon}$, which is nearly the same as the exact value (derived from the Wannier function integration with the $\sim 1/r$ operator) of 1.533 [9]. As we intend to systematically analyze the resulting order while increasing the maximal value of Z, we have computed V^Z up to $Z = 36$; however, in Fig. 1, we show data collected for maximal $Z = 12$ for the sake of clarity. Intriguingly, for $Z \in [2, 4]$, the classic $1/r$ potential is characterized by clearly lower values than those computed within Eq. (8). However, this directly arises from the fact that, in Eq. (8), the interactions are the sum of virtually *fractional* charges $e/3$, which are equally distributed among the vertices of the triangle. Nevertheless, for $Z \geq 8$, V^Z becomes nearly identical to the classical interaction between point charges e, as shown in Fig. 1. Note that parameters V^Z for the twist-angle 1.05° have also been elaborated with the inclusion of screening effects [11]. The estimates for U are ~ 15 meV (using the cRPA method); however, the ratio

U/V^Z remains of the same order, at least up to $Z = 12$, as for the data provided in Fig. 1. Therefore, we do not expect qualitative differences when compared to the values calculated by us.

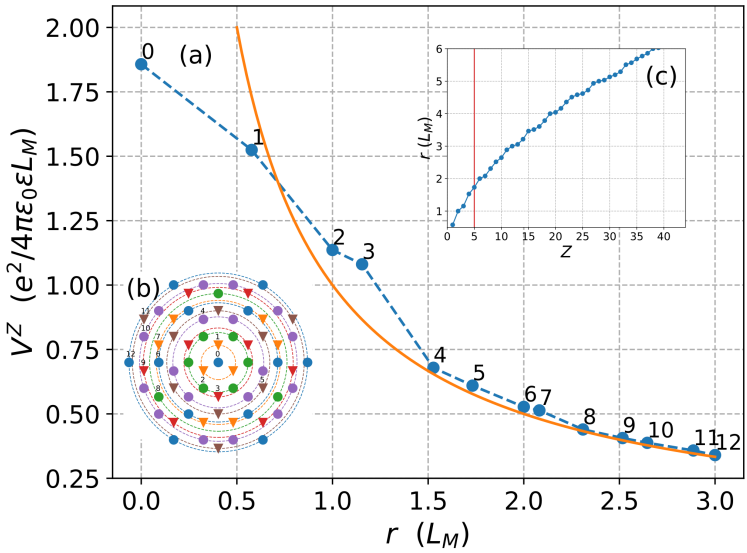

Fig. 1. (a) V^Z as a function of distance between sites obtained by means of Eq. (8) (blue circles). Numbers above the symbol refer to Z; the orange solid line is classical Coulomb potential $V(r) = \frac{1}{r}$ given for comparison; (b) coordination zones in the honeycomb lattice are presented; distance r given in L_M units as a function of Z in the honeycomb lattice.

3.2. Charge order

We have performed calculations for the lattice of size $12L_M \times 12L_M$ with the periodic boundary conditions assumed for both the UHF and semi-classical approach calculations. This size ensures that the maximum Z can be taken up to 36 to avoid multiple occurrence summations for the different Z for a given interaction (see Fig. 1 (c)). On the other hand, this size can be considered not too large; that is, the tendency towards the formation of anti-phase domains is reduced. In the SA-based case, we take the starting $\beta = 0.5$ and increment it by a value of 0.1 until convergence is reached. For each β, we perform 10^6 trials of configuration changes. We sweep $Z \in [3, 36]$ for SA and, as a cross-check, $Z \in [3, 12]$ in the UHF calculations. The convergence in the SA procedure is mostly achieved for $\beta \approx 1$–1.5.

By scanning maximal $Z^{\max} \in [3, 36]$ in the SA-based simulations, we have found that the resultant order depends on the range of interactions taken into account. However, we have observed that patterns appear repeatedly. Thus, we have selected four of them labeled I, II, III, and IV, which are present at least three times, as presented in Fig. 2. Note that for $Z^{\max} = 3$, that is, for the limit in which interactions cannot be treated as classical point charges directly, we have obtained the stripe order, which we assign as I (see Eq. (8)). This is identical to that reported by Klug *et al.* [12] also delivered using similar methods as applied in this study. Nevertheless, the increase in $Z^{\max}$, that is, the inclusion of interaction amplitudes that approach the classical limit $\sim 1/r$, results in the formation of different patterns (see Figs. 2 (b)–(c)). We find that selected types I, II, III, and IV appear 7, 6, 5, and 4 times, respectively, in the considered range of $Z^{\max}$. Other orders appear once or twice, or no evident pattern emerges. Importantly, we observed that in *each* pattern, lattice sites are preferably occupied by electrons in such a way that both valley orbitals referring to the given site are full, which is $n_{\nu,\xi} = 2$. Therefore, the total charge accumulated on the given site is $n_\mu = n_{\nu,\alpha} + n_{\nu,\beta} = 4$, and both the odd and $n_\mu = 2$ number of charges are, in practice, not present. We have cross-checked our results by

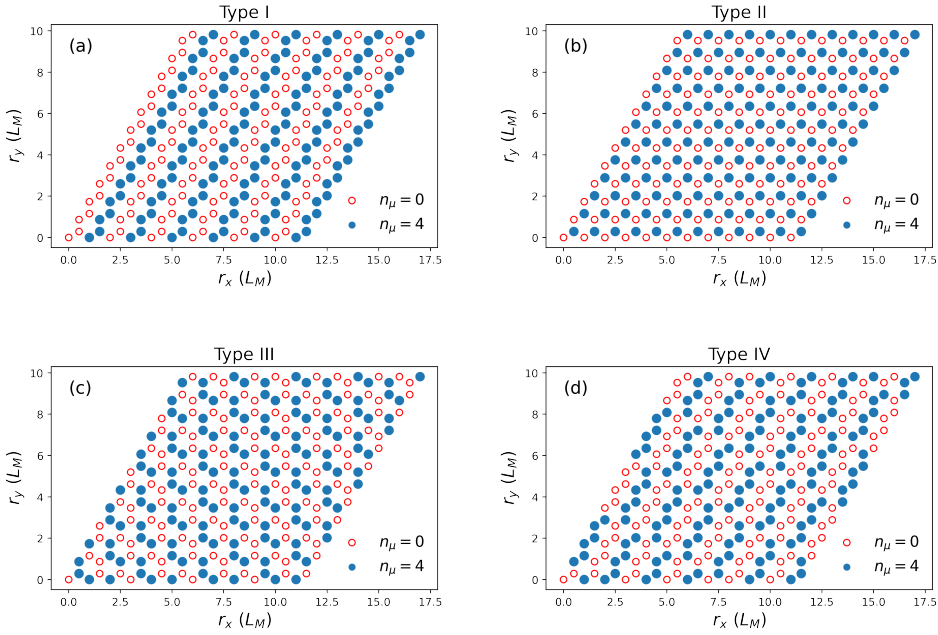

Fig. 2. Selected resultant orders from the SA simulations which appear repeatedly when increasing Z. Note that each site represents two valley orbitals, thus the total charge can be up to 4. We assign these orders as I (a), II (b), III (c), and IV (d).

means of UHF calculation for $Z^{\max}$ up to 12, obtaining the identical pattern for each case when compared to those collected by the application of our *semi-classical* approach.

Since we have not obtained *saturation* in the sense that one type of order stabilizes with increasing $Z^{\max}$, we decided to perform the analysis based on the energy and the resulting order. In Fig. 3, the total energy in units of $E^{Z_{\max}} = 3$ is shown. One finds that the energy obtained from

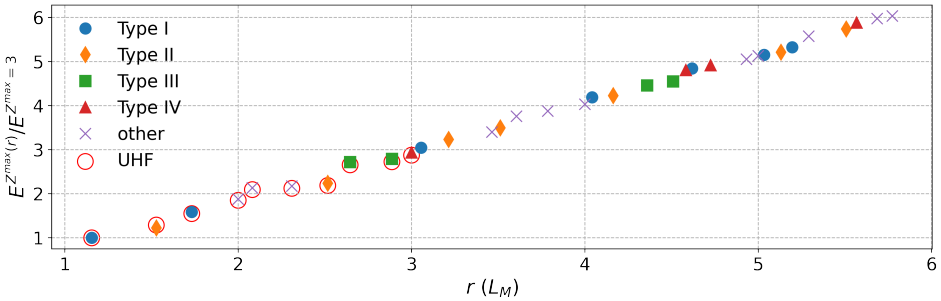

Fig. 3. Energy collected for the $12L_M \times 12L_M$ system, in the units of energy obtained for $Z^{\max} = 3$. Different symbols are prescribed to the selected type of order which repeat when $Z^{\max}$ increases. The agreement between the UHF (hollow circles) and SA-based approach is nearly perfect at least up to $Z^{\max} = 12$ as can be deduced.

the UHF calculations nearly exactly fits the respective values coming from SA, which validates our assumptions when establishing the semi-classical model. As can be deduced from the data presented in Fig. 3, the energy seems to behave linearly. This observation is not astonishing, since although we simulate TBG for the charge-neutral case ($\nu = 0$), the effective model *is not*, and the energy with increasing cut-off radius encoded in $Z^{\max}$ diverges as $\sim r$ (see *e.g.* Ref. [33]). However, as some types of orders repeat, we decided to perform a kind of *poor man* analysis; that is, to investigate the magnitude of divergence while taking into account all data collected and considering each selected type separately. Namely, we perform the linear fit

$$E_T^{Z^{\max}(r)} \Big/ E_T^{Z^{\max}=3} = a_T \times r + b_T \,, \tag{9}$$

where $T \in \{\text{Type I}, \text{Type II}, \text{Type III}, \text{Type IV}, \text{other}, \text{all}\}$ and subsequently analyze

$$\Delta a_T \equiv (a_T - a_{\text{all}}) \times r \,, \tag{10}$$

as we are interested in the rate of divergence for each type when compared to the overall tendency with increasing $Z^{\max}$. In Fig. 4, we visualize our

findings in this regard by plotting $\Delta a_r \times r$ while taking into account the errors of the fits. As can be deduced, the ratios of energy divergence related to Type I and Type III are characterized by a lower magnitude than the fit to all data points (since $\Delta a_{\text{all}} \equiv 0$). However, Type III undoubtedly exposes the lowest ratio. Additionally, we find that the energies of Type II and Type IV diverge substantially faster. On the other hand, non-qualified orders taken collectively seem to behave similarly to the overall tendency (disregarding the type of order).

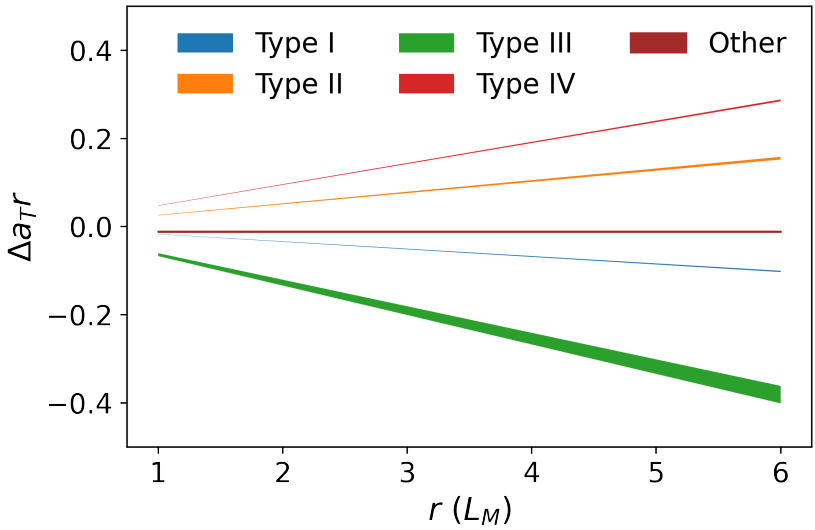

Fig. 4. Selected resultant orders from SA simulations which appear repeatedly when increasing Z. Note that each site represents two valley orbitals, thus the total charge can be up to 4. We assign these orders as I (a), II (b), III (c), and IV (d).

4. Summary

In this report, we have analyzed the charge order in the low-energy Hubbard-like model describing the twisted bilayer graphene system at a twist angle $\phi = 1.05°$. As a main method, we have used an optimization algorithm based on the Simulated Annealing procedure for the *semi-classical* model, similarly to Ref. [12]. The validity of the approach has been proven by independent unrestricted Hartree–Fock method calculations. We show that the resulting charge pattern in the honeycomb lattice, equipped with two valley degrees of freedom, depends on the range of density–density interactions taken into account. However, we have identified patterns that repeat when the range of interaction is systematically increased. Three of

them are of *stripe* character. By performing the study of the energy divergence concerning each type of pattern separately, we designate two types of stripe-ordering whose energy divergence rate is lower than the trend related to the whole patterns taken collectively.

Naturally, this kind of analysis cannot be considered the definitive indicator of the ultimate pattern of order; it suggests that it may differ from that which pertains to the inclusion of density–density interactions, limited only to those belonging to the non-classical regime, that is, for $Z^{\max} = 3$. Precisely, Type III of order differs by possessing three fully occupied lattice sites resembling *a banana-like stripe primitive cell*, which periodically repeats in each stripe instead of two fully occupied sites in Type I, previously reported [12].

Although our conclusions can hardly be considered the ultimate answer to what kind of order in TBG for the neutrally charged case dominates, we at least provide a possible candidate in this regard. We look forward to seeing both the experimental and theoretical progress concerning this issue, which will confirm or deny the predictions made by us.

This research was funded by the National Science Centre (NCN), Poland according to decision 2021/42/E/ST3/00128. We gratefully acknowledge Poland's high-performance Infrastructure PLGrid ACK Cyfronet AGH for providing computer facilities and support within the computational grant No. PLG/2025/018169.

I would like to express my special thanks to Professor Józef Spałek and Dr. Leszek Spałek, thanks to whom this and my other works in the field of correlated electron systems could be created.

REFERENCES

[1] E.Y. Andrei *et al.*, «The marvels of moiré materials», *Nat. Rev. Mater.* **6**, 201 (2021).

[2] E.Y. Andrei, A.H. MacDonald, «Graphene bilayers with a twist», *Nat. Mater.* **19**, 1265 (2020).

[3] Y. Cao *et al.*, «Correlated insulator behaviour at half-filling in magic-angle graphene superlattices», *Nature* **556**, 80 (2018).

[4] Y. Cao *et al.*, «Unconventional superconductivity in magic-angle graphene superlattices», *Nature* **556**, 43 (2018).

[5] H.C. Po, L. Zou, A. Vishwanath, T. Senthil, «Origin of Mott Insulating Behavior and Superconductivity in Twisted Bilayer Graphene», *Phys. Rev. X* **8**, 031089 (2018).

[6] M. Oh *et al.*, «Evidence for unconventional superconductivity in twisted bilayer graphene», *Nature* **600**, 240 (2021).

[7] D. Bennett *et al.*, «Twisted bilayer graphene revisited: Minimal two-band model for low-energy bands», *Phys. Rev. B* **109**, 155422 (2024).

[8] R. Bistritzer, A.H. MacDonald, «Moiré bands in twisted double-layer graphene», *Proc. Natl. Acad. Sci.* **108**, 12233 (2011).

[9] M. Koshino *et al.*, «Maximally Localized Wannier Orbitals and the Extended Hubbard Model for Twisted Bilayer Graphene», *Phys. Rev. X* **8**, 031087 (2018).

[10] X. Lin, D. Tománek, «Minimum model for the electronic structure of twisted bilayer graphene and related structures», *Phys. Rev. B* **98**, 081410 (2018).

[11] Z.A.H. Goodwin, F. Corsetti, A.A. Mostofi, J. Lischner, «Attractive electron–electron interactions from internal screening in magic-angle twisted bilayer graphene», *Phys. Rev. B* **100**, 235424 (2019).

[12] M.J. Klug, «Charge order and Mott insulating ground states in small-angle twisted bilayer graphene», *New J. Phys.* **22**, 073016 (2020).

[13] X.Y. Xu, K.T. Law, P.A. Lee, «Kekulé valence bond order in an extended Hubbard model on the honeycomb lattice with possible applications to twisted bilayer graphene», *Phys. Rev. B* **98**, 121406 (2018).

[14] B.-B. Chen *et al.*, «Realization of topological Mott insulator in a twisted bilayer graphene lattice model», *Nat. Commun.* **12**, 5480 (2021).

[15] Y. Da Liao *et al.*, «Correlation-Induced Insulating Topological Phases at Charge Neutrality in Twisted Bilayer Graphene», *Phys. Rev. X* **11**, 011014 (2021).

[16] N.F.Q. Yuan, L. Fu, «Model for the metal–insulator transition in graphene superlattices and beyond», *Phys. Rev. B* **98**, 045103 (2018).

[17] M. Fidrysiak, M. Zegrodnik, J. Spałek, «Unconventional topological superconductivity and phase diagram for an effective two-orbital model as applied to twisted bilayer graphene», *Phys. Rev. B* **98**, 085436 (2018).

[18] G. Shavit, E. Berg, A. Stern, Y. Oreg, «Theory of Correlated Insulators and Superconductivity in Twisted Bilayer Graphene», *Phys. Rev. Lett.* **127**, 247703 (2021).

[19] T. Devakul, V. Crépel, Y. Zhang, L. Fu, «Magic in twisted transition metal dichalcogenide bilayers», *Nat. Commun.* **12**, 6730 (2021).

[20] X. Lu *et al.*, «Superconductors, orbital magnets and correlated states in magic-angle bilayer graphene», *Nature* **574**, 653 (2019).

[21] E.C. Regan *et al.*, «Mott and generalized Wigner crystal states in WSe_2/WS_2 moiré superlattices», *Nature* **579**, 359 (2020).

[22] H. Li *et al.*, «Imaging two-dimensional generalized Wigner crystals», *Nature* **597**, 650 (2021).

[23] T. Li *et al.*, «Continuous Mott transition in semiconductor moiré superlattices», *Nature* **597**, 350 (2021).

[24] Y. Tang *et al.*, «Dielectric catastrophe at the Wigner–Mott transition in a moiré superlattice», *Nat. Commun.* **13**, 4271 (2022).

[25] H. Pan, F. Wu, S. Das Sarma, «Band topology, Hubbard model, Heisenberg model, and Dzyaloshinskii–Moriya interaction in twisted bilayer WSe_2», *Phys. Rev. Res.* **2**, 033087 (2020).

[26] J. Motruk, D. Rossi, D.A. Abanin, L. Rademaker, «Kagome chiral spin liquid in transition metal dichalcogenide moiré bilayers», *Phys. Rev. Res.* **5**, L022049 (2023).

[27] M. Zegrodnik, A. Biborski, «Mixed singlet-triplet superconducting state within the moiré t–J–U model applied to twisted bilayer WSe_2», *Phys. Rev. B* **108**, 064506 (2023).

[28] P. Saha, L. Rademaker, M. Zegrodnik, «Interplay between topology and electron–electron interactions in the moiré $MoTe_2/WSe_2$ heterobilayer», *Phys. Rev. B* **112**, 045147 (2025).

[29] A. Biborski, M. Zegrodnik, «Signatures of superconducting pairing driven by electron–electron interactions in moiré WSe_2/WSe_2 homobilayer modeled by Hubbard Hamiltonian», *Phys. Rev. B* **112**, L161122 (2025).

[30] A. Biborski, M. Zegrodnik, «Charge and spin properties of a generalized Wigner crystal realized in the moiré WSe_2/WS_2 heterobilayer», *Phys. Rev. B* **111**, 075116 (2025).

[31] T. Misawa *et al.*, «mVMC — Open-source software for many-variable variational Monte Carlo method», *Comput. Phys. Commun.* **235**, 447 (2019).

[32] R. Bessler, U. Duerig, E. Koren, «The dielectric constant of a bilayer graphene interface», *Nanoscale Adv.* **1**, 1702 (2019).

[33] V. Ballenegger, A. Arnold, J.J. Cerdà, «Simulations of non-neutral slab systems with long-range electrostatic interactions in two-dimensional periodic boundary conditions», *J. Chem. Phys.* **131**, 094107 (2009).